Supporting Information:

General strategy for doping rare earth metals into Au-ZnO core-shell nanospheres

René Zeto, Daniel Cummins, Arynn Gallegos, Mike Shao, Andrea M. Armani

Contents

Pre-calcine particle analysis

Dynamic Light Scattering (DLS) characterization

DLS is used to analyze the size distribution of nanoparticles with and without a gold core and the size distribution of nanoparticles doped with Cu ranging from 2-10%. All data is plotted in Figures S1-S2. In general, the size distribution is narrower when the gold core is present (Figure S3). The size distributions for particles without an Au core were broader, as can be seen in Figures S1 and S2. This is also reflected in their higher polydispersity index (PDI) values. Particles with a gold core had PDI values that were ~10% lower, on average, than the particles without a gold core (Figure S3).

In the cases where particle diameters significantly lower than ~120 nm were picked up by DLS, we believe that the DLS instrument was detecting gold cores. Due to the constraints of the shell growth conditions, we used an excess of gold cores, thus, not every core formed a shell. Additionally, in some spectra, a second peak in the 1-10 μm range was present and was attributed to solution debris as all particles in the SEM imaging were under 1 μm. For this reason, the secondary peaks indicating particles larger 1 μm in size were excluded from calculation of the average particle sizes and PDI values.

We also measured the size distributions of the particles doped with rare earth metals. Size distributions were obtained via DLS for particles doped at 1% with every element used in this study (Figure S4).

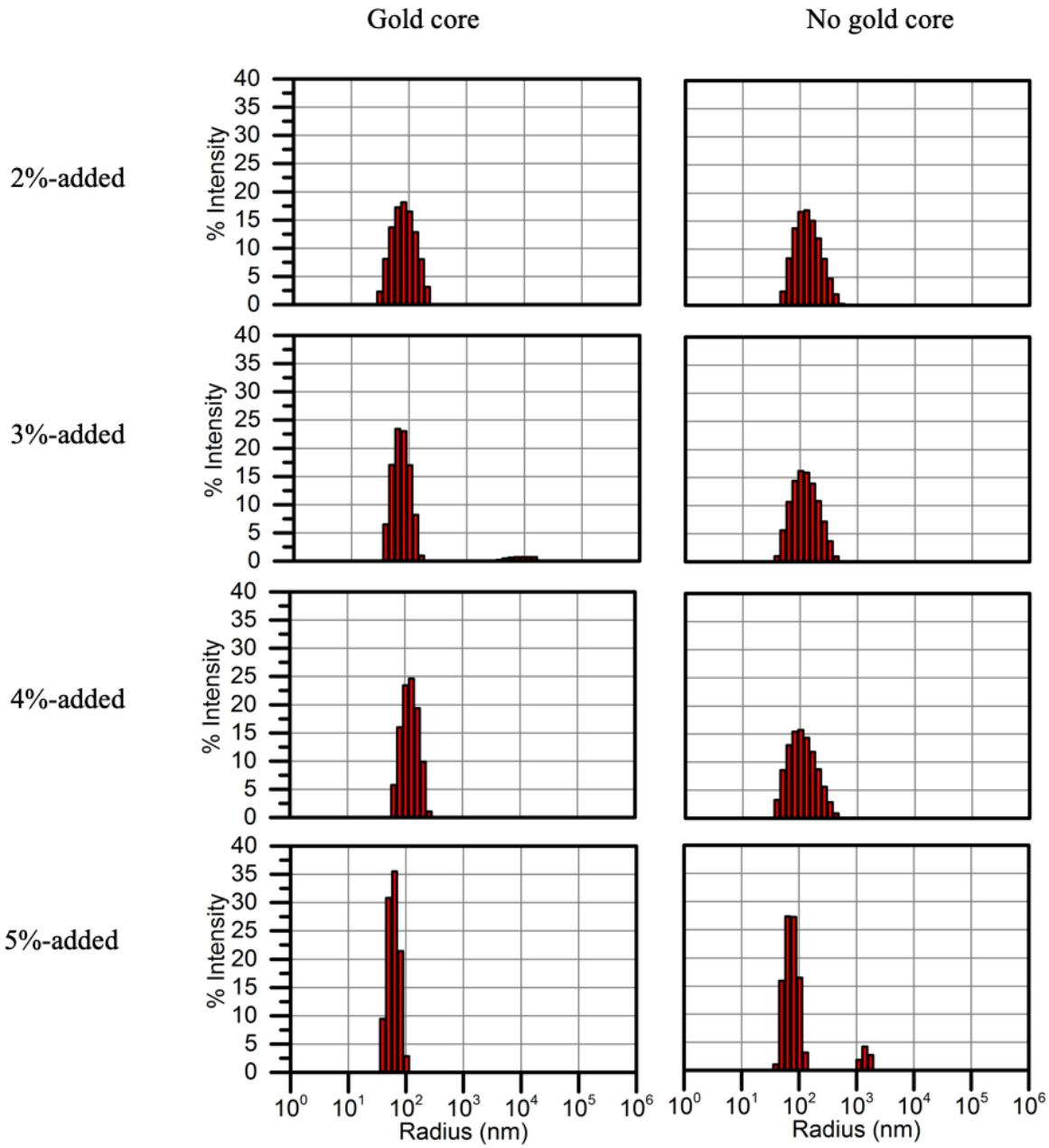

FIG. S1: DLS scans for nanoparticles with 2-5%-added Cu added to the Zn-based shell layer, with gold core (left column) and without gold core (right column).

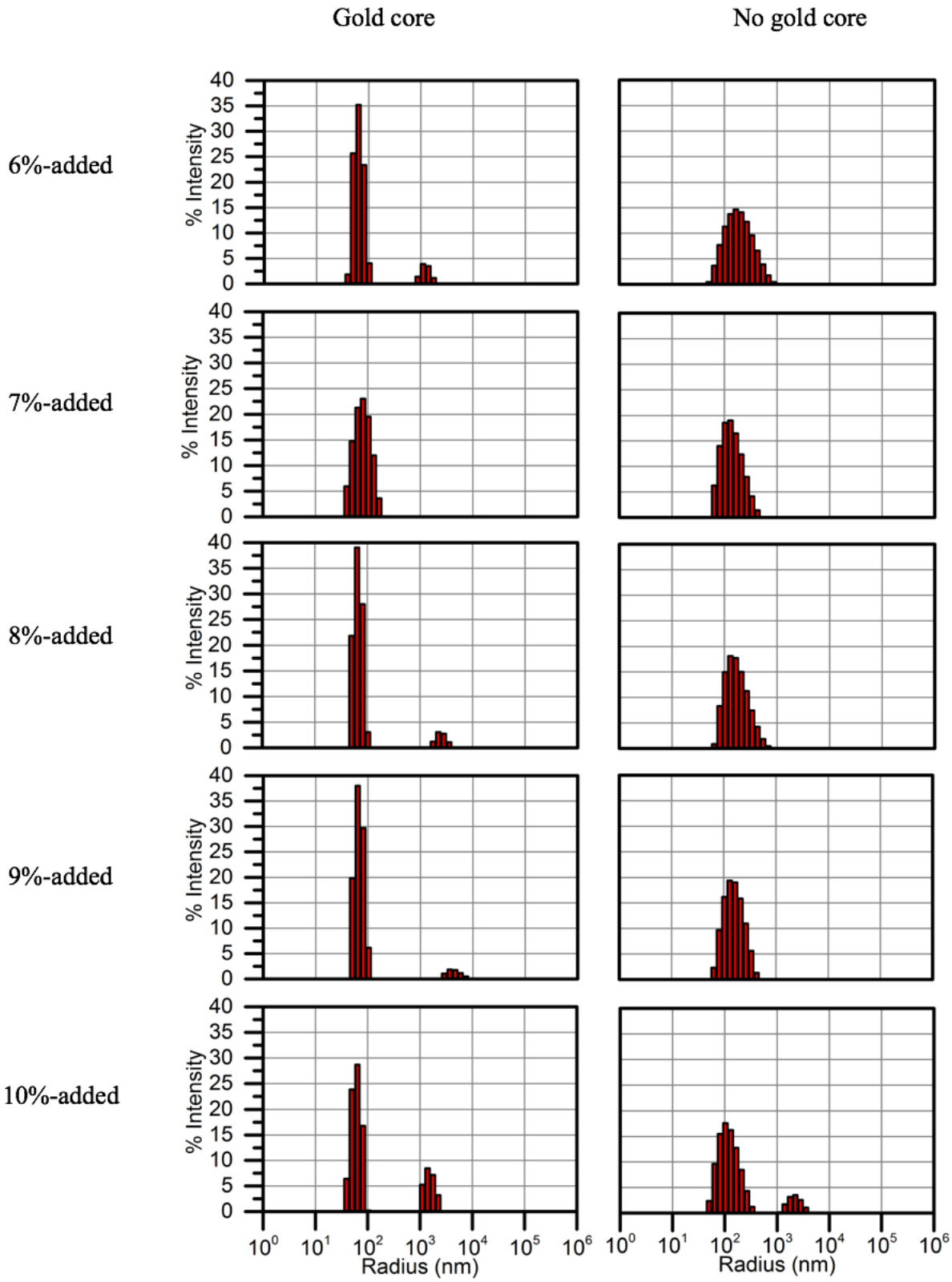

FIG. S2: DLS scans for nanoparticles with 6-10%-added Cu to the Zn-based shell layer, with gold core (left column) and without gold core (right column).

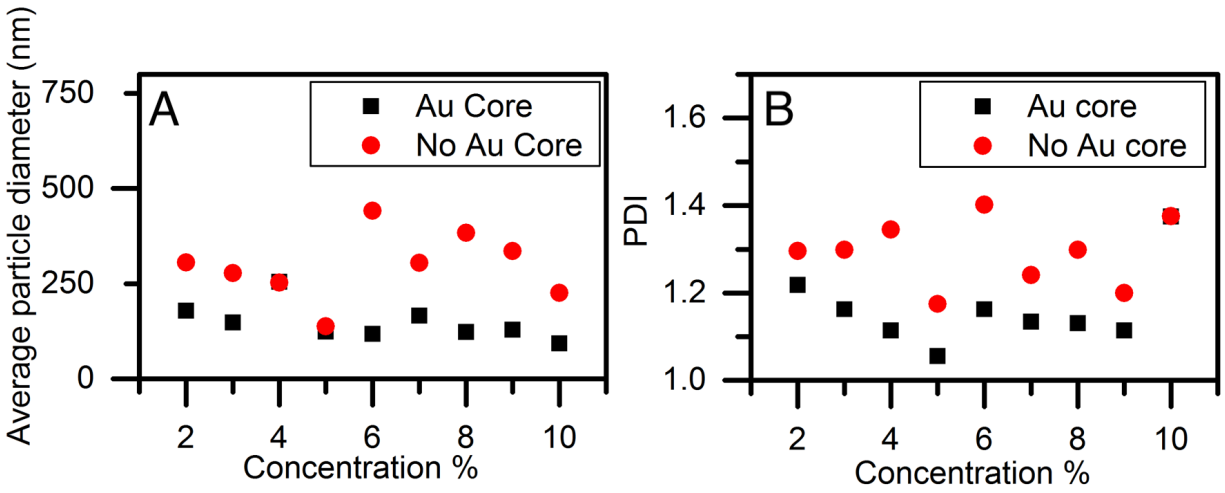

FIG. S3: A) Average particle diameters of the same samples. B) Polydispersity index (PDI) determined from DLS results for particles with different Cu concentrations with and without a gold core, across a range of dopants. The gold core resulted in enhanced monodispersity that was maintained regardless of the dopant used.

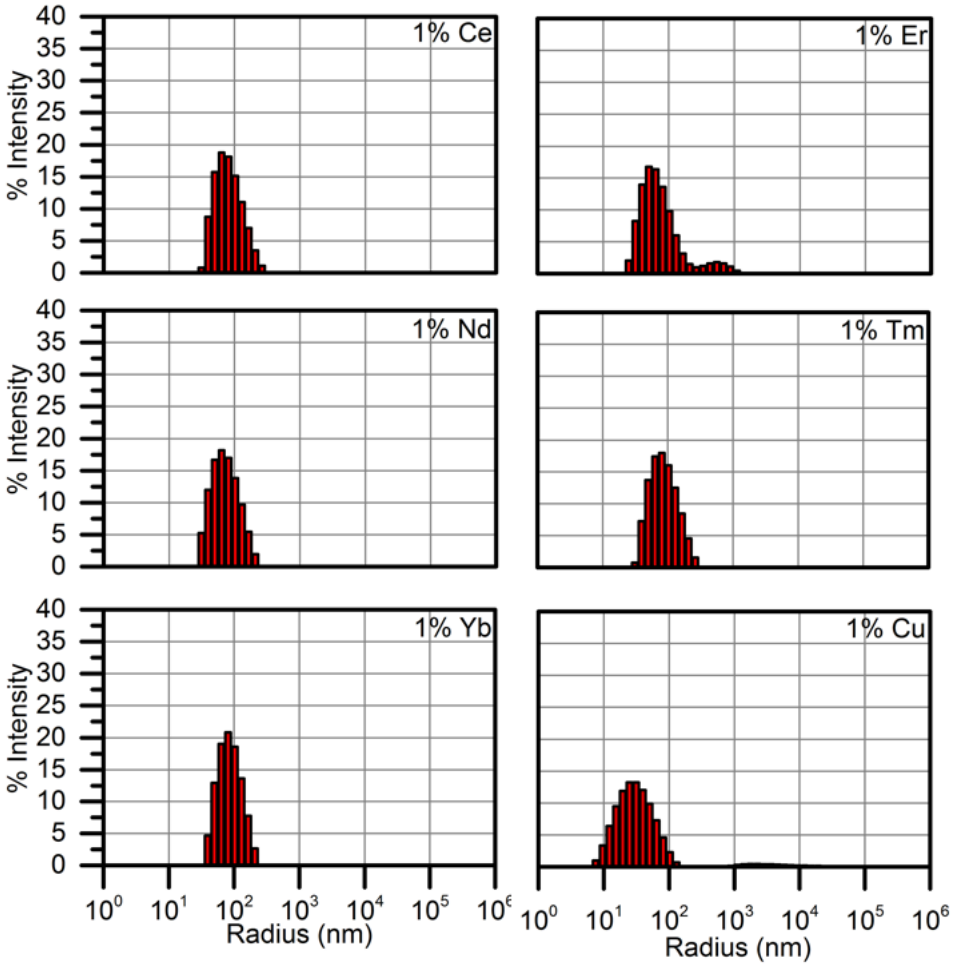

FIG. S4: DLS scans for additional dopants at 1% concentrations, showing uniformity across dopants at fixed concentration. All nanoparticles contain gold cores.

Electron microscopy analysis

SEM-EDX imaging and analysis

Before SEM-EDX analysis, the particles were thoroughly washed via centrifugation, removing any precursor dopant ions not incorporated into the particles. After washing, a 10 μL sample of each type of doped particles was deposited onto a separate Si/SiO_2 wafer piece and left to dry at 60 °C for 10 minutes. The SEM used was an FEI Nova NanoSEM, equipped with a ThermoFisher UltraDry 100 mm^2 Windowless EDS. The EDX spectra were typically obtained at a 20 kV accelerating voltage, which provides good signal intensity. SEM imaging was performed in parallel.

Representative images are presented in Figures S5-S10. These images confirm the synthesis and the core-shell particle structure. Additionally, while the general spherical morphology of the particle appears uniform in the low doping concentration regime (1-6%), perturbations to this shape can begin to be seen at higher relative mol% concentrations, such as in 6% for Nd.

The samples analyzed using EDX are bulk aggregates of pre-calcine particles doped at 1%, similar to the particles shown in Figure S5-S10.

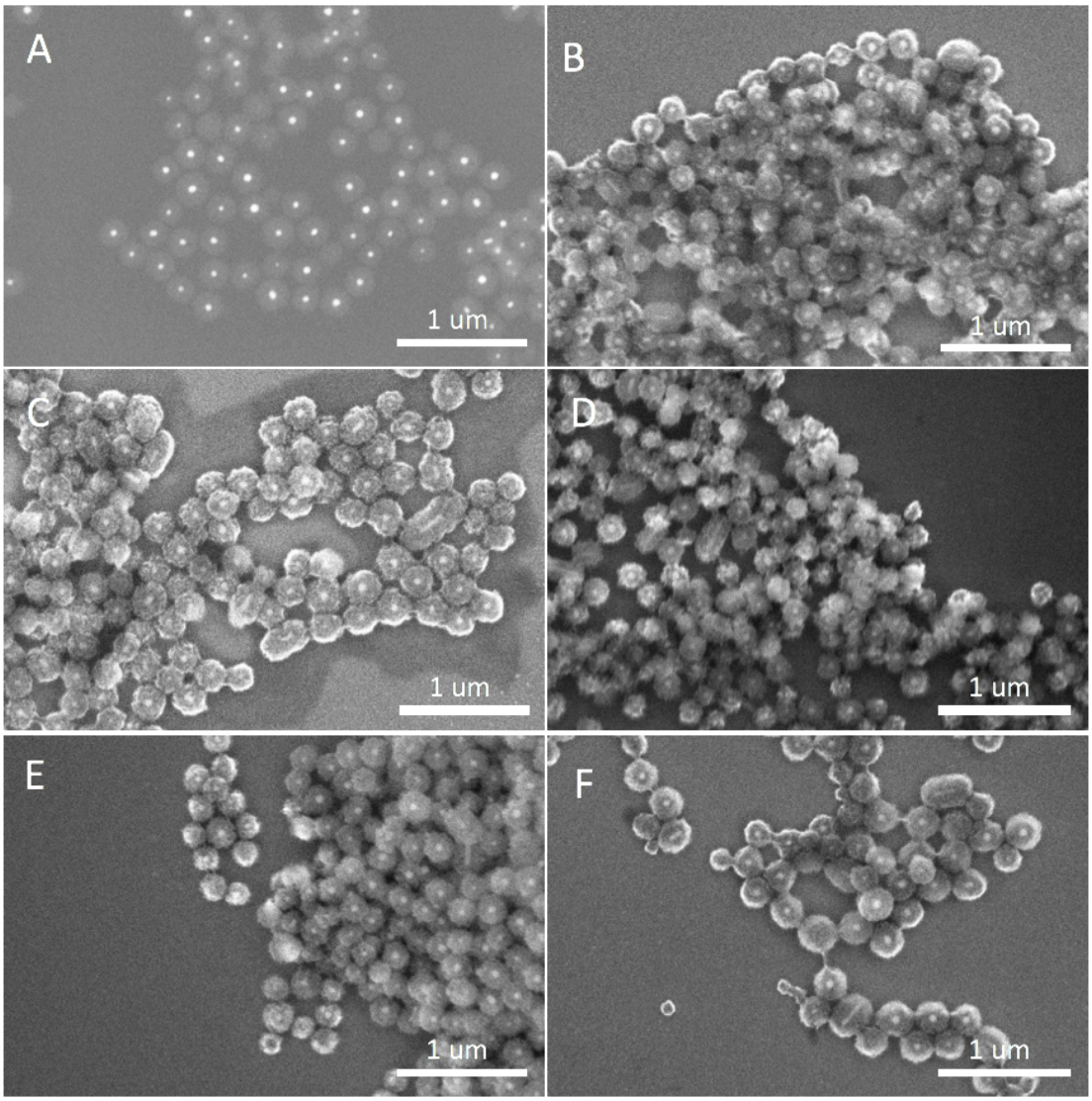

FIG. S5: Scanning electron microscope (SEM) images verifying core-shell nanoparticle formation for Cu-doped core-shell particles at: A) 1%, B) 2%, C) 3%, D) 4%, E) 5%, and F) 6%-added concentrations of Cu. The ZnO shell clearly encapsulates the gold core in all images.

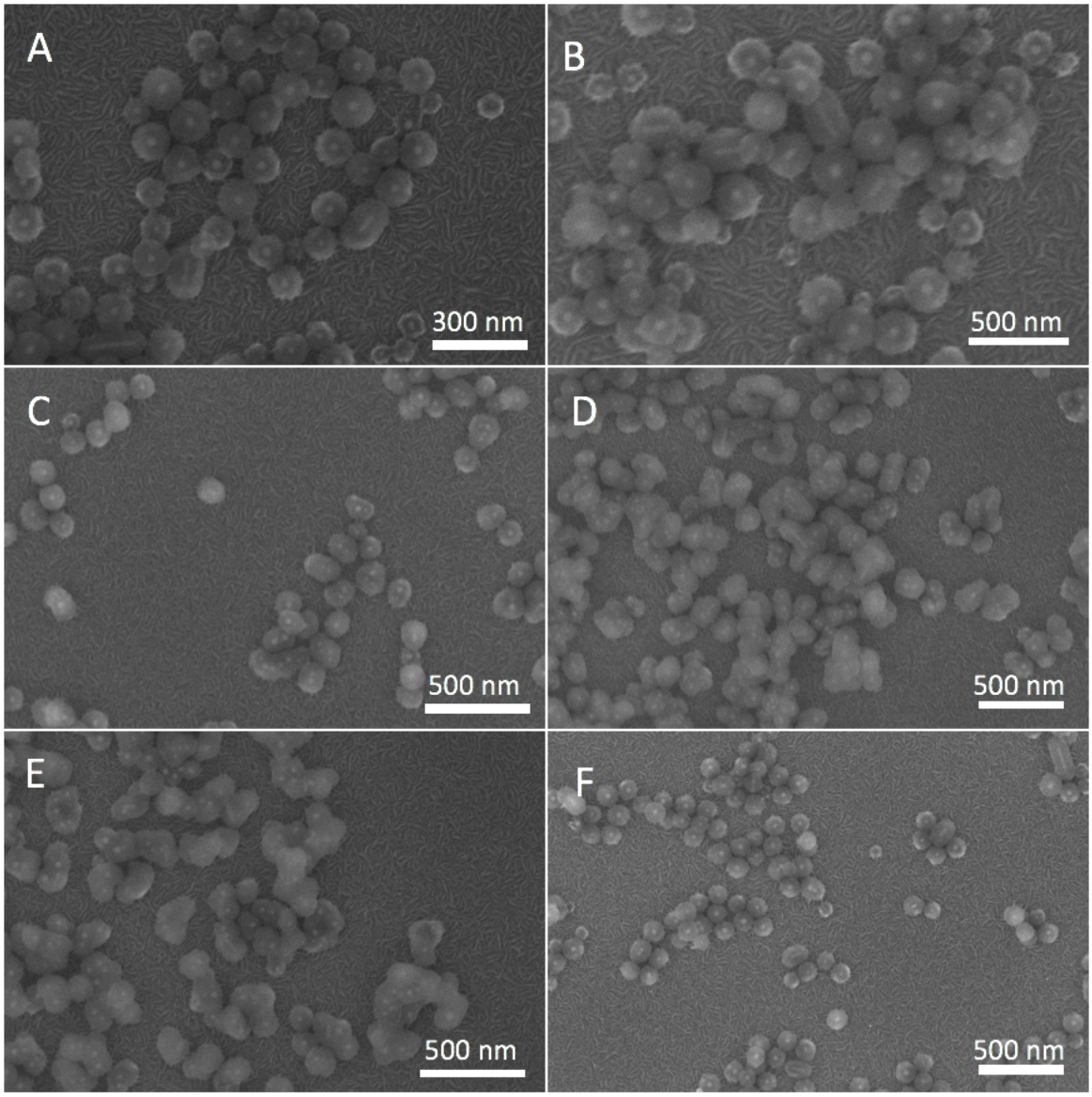

FIG. S6: Scanning electron microscope (SEM) images verifying core-shell nanoparticle formation for Ce-doped core-shell particles at: A) 1%, B) 2%, C) 3%, D) 4%, E) 5%, and F) 6%-added concentrations of Ce. The ZnO shell clearly encapsulates the gold core in all images.

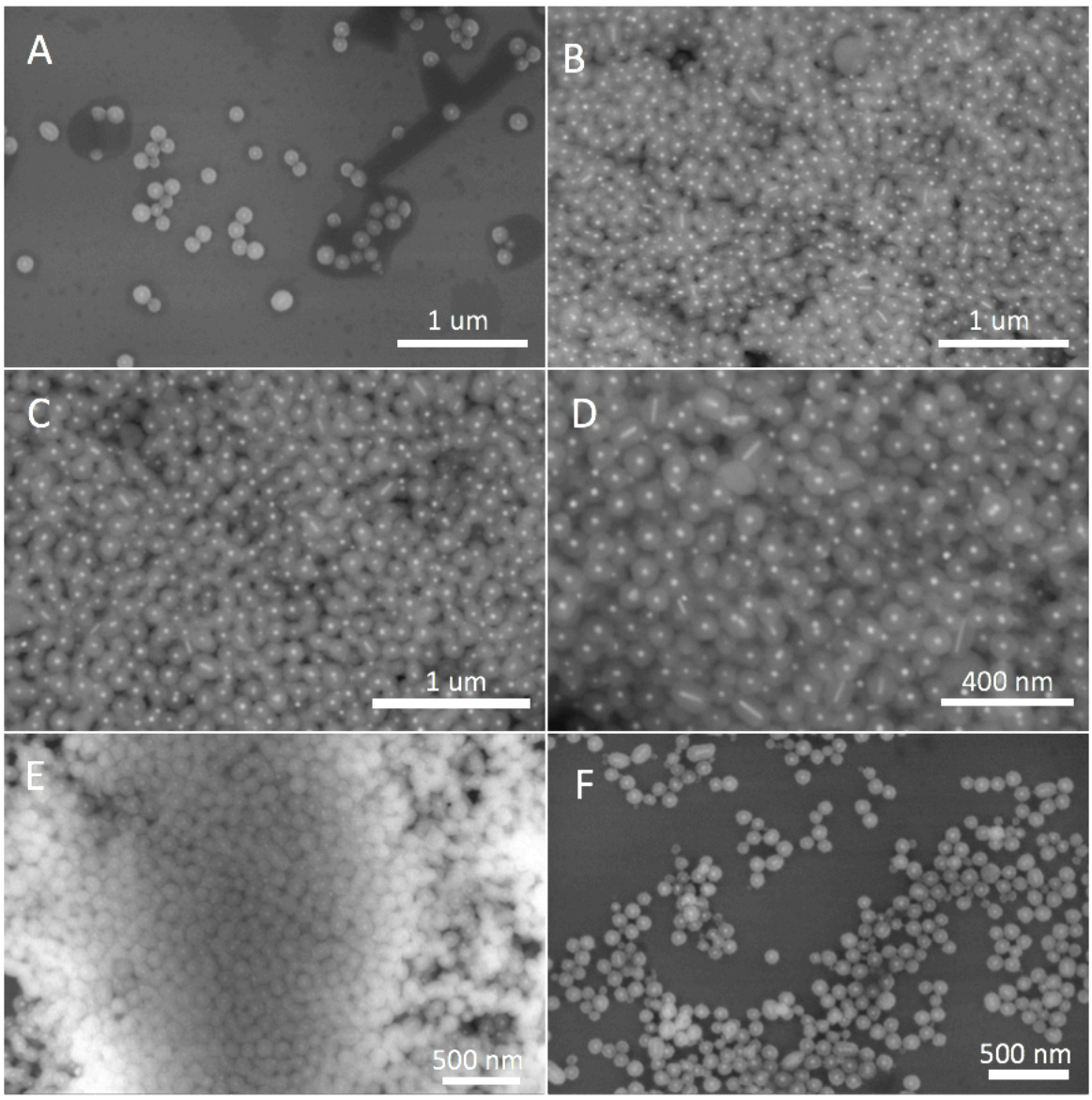

FIG. S7: Scanning electron microscope (SEM) images verifying core-shell nanoparticle formation for Er-doped core-shell particles at: A) 1%, B) 2%, C) 3%, D) 4%, E) 5%, and F) 6%-added concentrations of Er. The ZnO shell clearly encapsulates the gold core in all images.

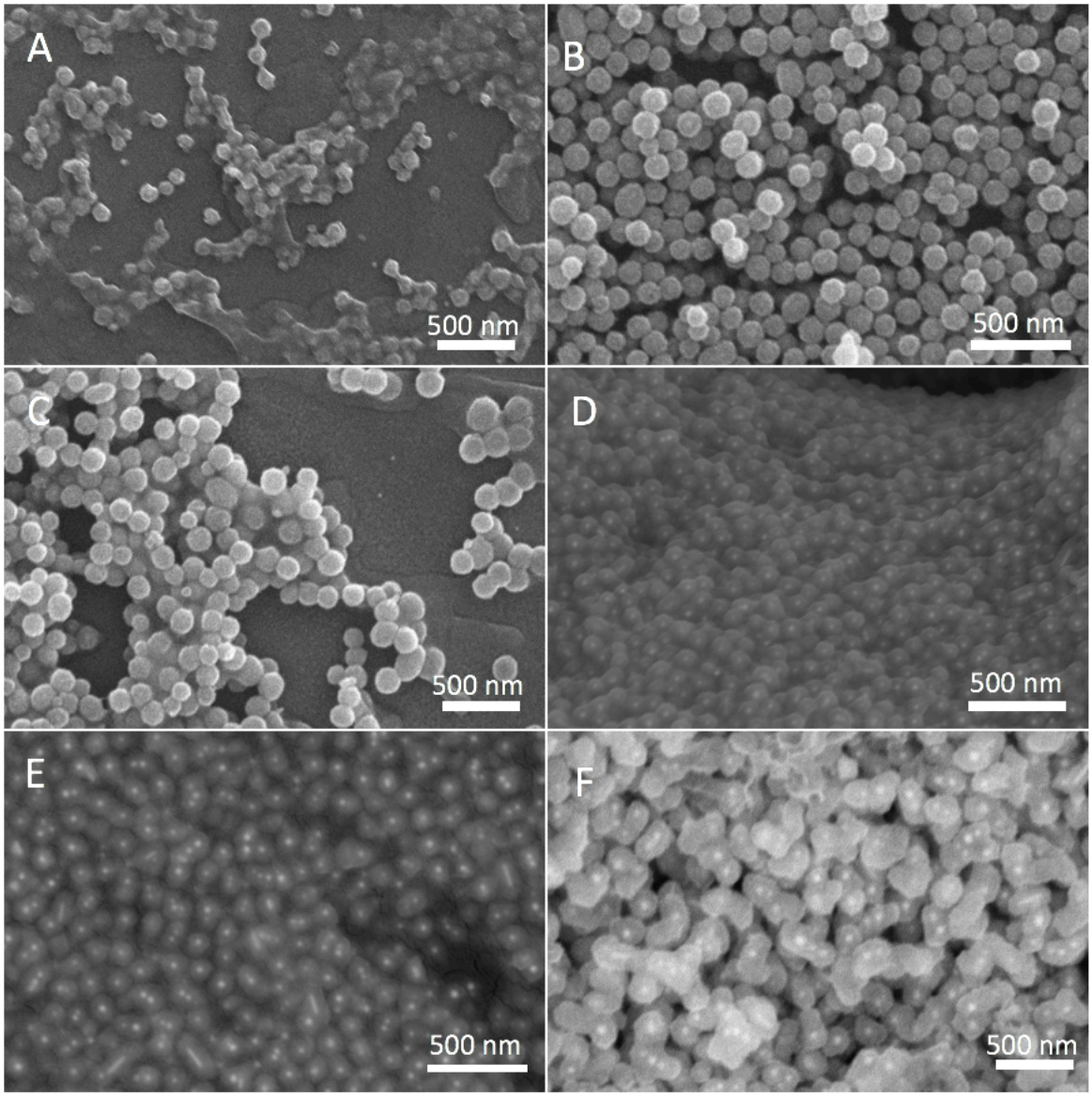

FIG. S8: Scanning electron microscope (SEM) images verifying core-shell nanoparticle formation for Nd-doped core-shell particles at: A) 1%, B) 2%, C) 3%, D) 4%, E) 5%, and F) 6%-added concentrations of Nd. The ZnO shell clearly encapsulates the gold core in all images.

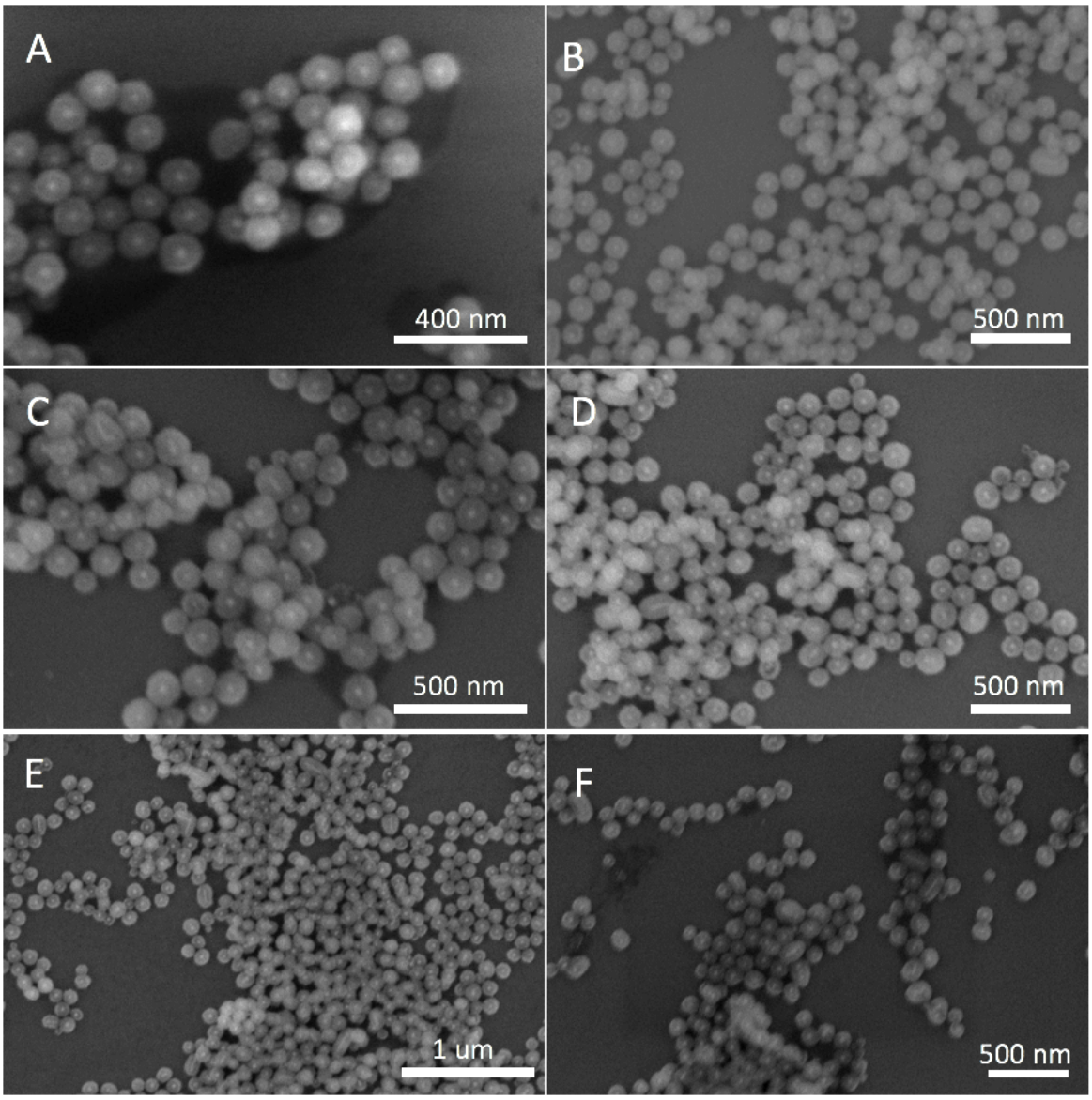

FIG. S9: Scanning electron microscope (SEM) images verifying core-shell nanoparticle formation for Tm-doped core-shell particles at: A) 1%, B) 2%, C) 3%, D) 4%, E) 5%, and F) 6%-added concentrations of Tm. The ZnO shell clearly encapsulates the gold core in all images.

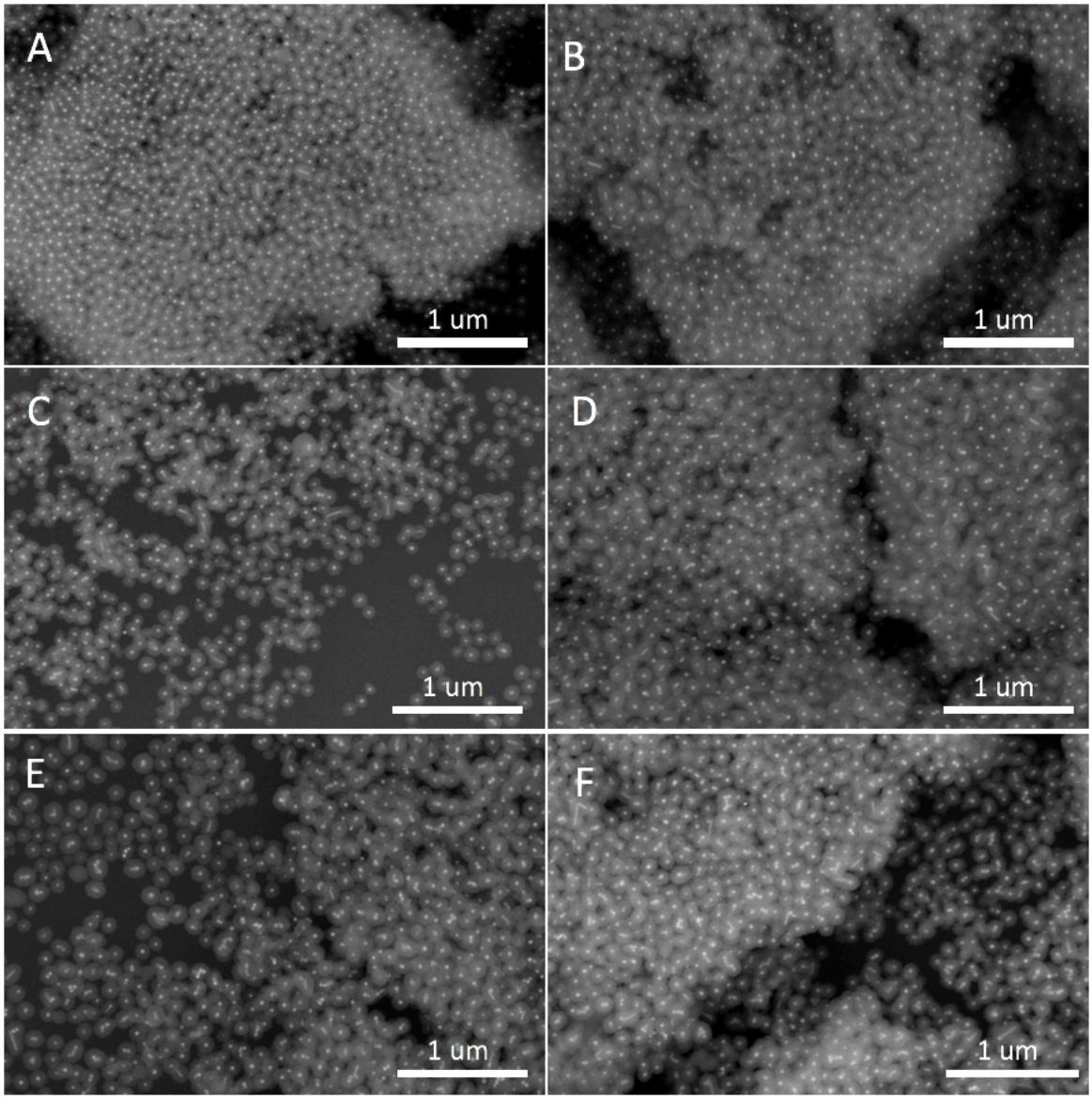

FIG. S10: Scanning electron microscope (SEM) images verifying core-shell nanoparticle formation for Yb-doped core-shell particles at: A) 1%, B) 2%, C) 3%, D) 4%, E) 5%, and F) 6%-added concentrations of Yb. The ZnO shell clearly encapsulates the gold core in all images.

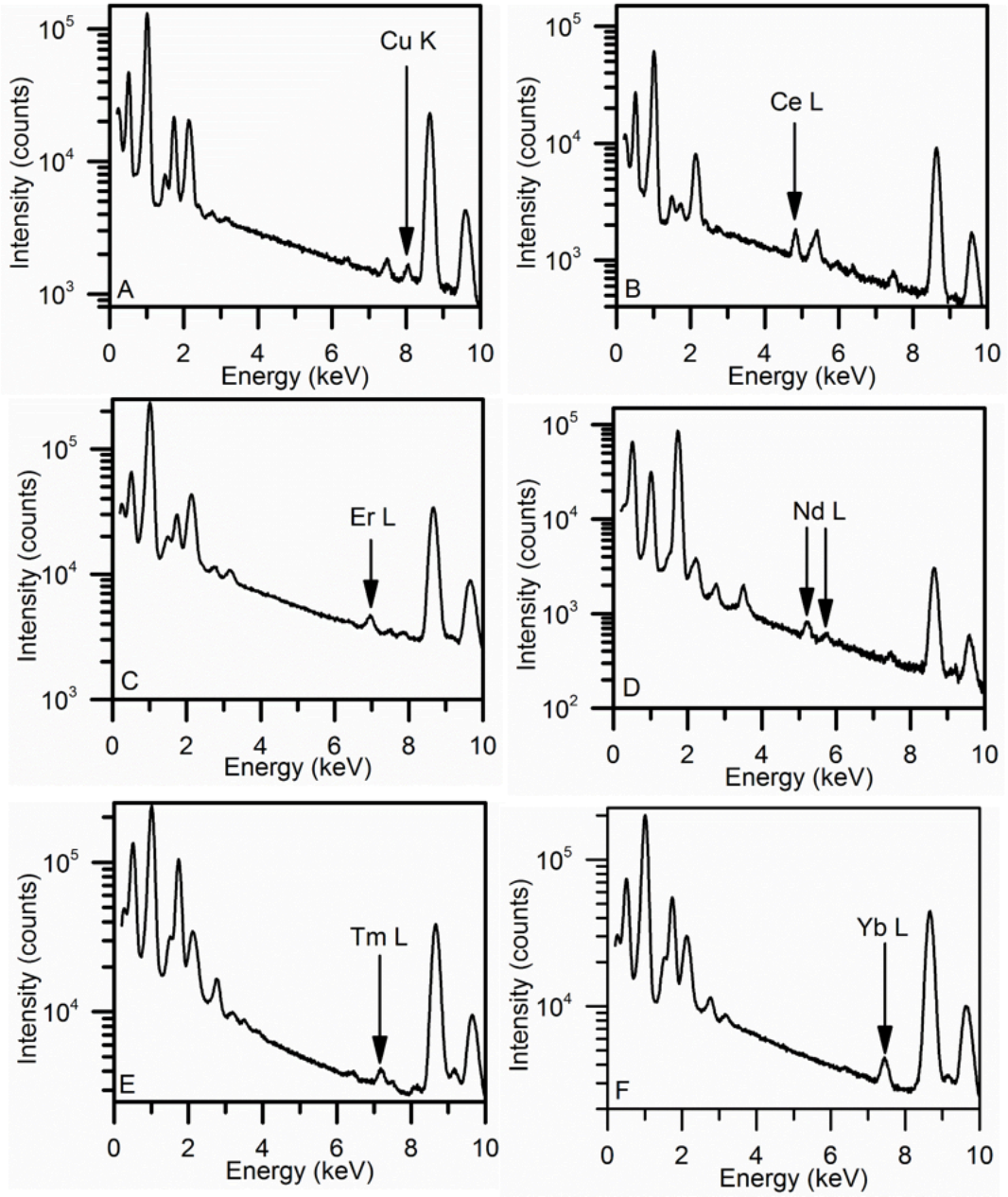

FIG. S11: EDX spectra of an aggregate of core-shell nanoparticles with: A) Cu, B) Ce, C) Er, D) Nd, E) Tm, and F) Yb-doped at 1% dopant concentration. These are representative spectra which confirm the presence of the dopant atom in the nanosphere.

With the exception of Cu, all six dopants represented in the EDX spectra of Figure S11 were detectable by their L transitions. For Cu, the K transition was strongest. In Figure S11, the lines detected were: Cu K at 8.04 keV, Ce L at 4.84 keV, Er L at 6.95 keV, Nd L at 5.23 keV, Tm L at 7.18 keV, and Yb L at 7.41 keV. Other peaks are present in the spectra of Figure S11, notably in the low energy (<4 keV) portion of the spectra. These peaks are all known, and attributable to the Si substrate, the Au core, and the Zn present in the shell, as well as various lighter elements such

as C, O, and N present both in the particles and as common contaminants in the chamber. On the higher energy portion of the spectra, two intense peaks are present: Zn K at 8.63 keV, and Au L at 9.71 keV. Thus, there is an empty middle portion of the spectra which provided an opportunity to detect the dopant atoms at concentrations as low as 1%.

TEM-EDX imaging and dopant characterization

To analyze the dopant distribution at the single particle level, TEM-EDX was used. Samples were prepared by depositing 10 μL of centrifuge-washed nanoparticle solution onto a SiN TEM grid and left to dry on a hot plate at 35 °C (in air). The dopant in the shell was 4%. Imaging was performed on the JEOL JEM-2100F TEM in STEM mode at 200 kV.

Clear spatial correlation between Zn and the dopant atom was seen for all dopants that were spectrally resolvable (Figure S12-S15). L lines were resolved for Ce, Nd, and Yb, and M lines for Tm and Yb. The Tm L line was not resolvable as it overlaps with the strong Co line at around 7 keV, and the M lines are located in the lower energy portion of the spectra, which has many background lines which are difficult to reliably deconvolve. Ce and Nd spatial maps are presented at higher definition 512x512 pixel resolution, and Tm and Yb at 128x128 for contrast. While all spatial maps were digitally enhanced to improve visual contrast, the qualitative conclusions regarding the spatial correlation is not affected.

Unfortunately, the Cu and Er dopants were unable to be detected using this method due to the presence of Cu and Co in the chamber. The background signal from the column Cu was larger than the particle Cu, and the Co lines overlapped with the Er lines.

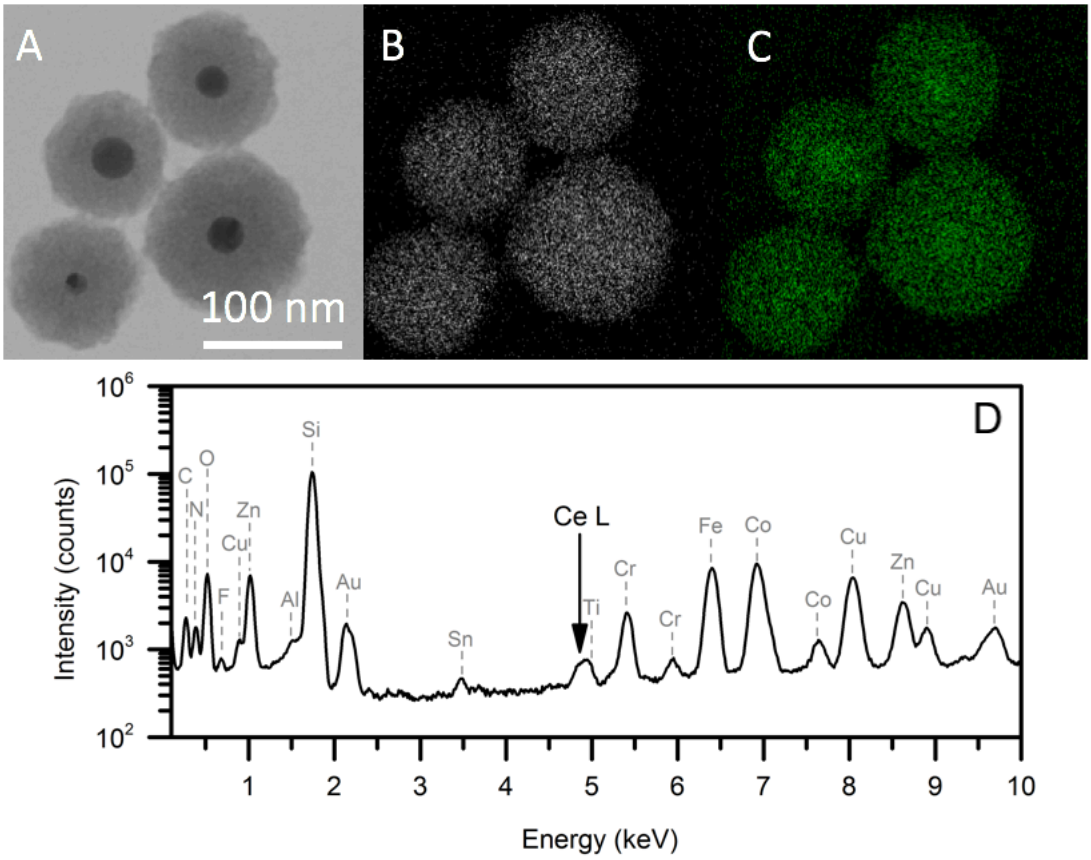

FIG. S12: Spatial correlation EDX-TEM for Ce-doped particles (pre-calcine) at 4%-added concentration (512x512). A) Greyscale TEM image, B) Spatial EDX map for Zn, C) Spatial EDX map for Ce. Color scale is enhanced for visual contrast in print. D) The corresponding spectrum, showing the presence of Ce.

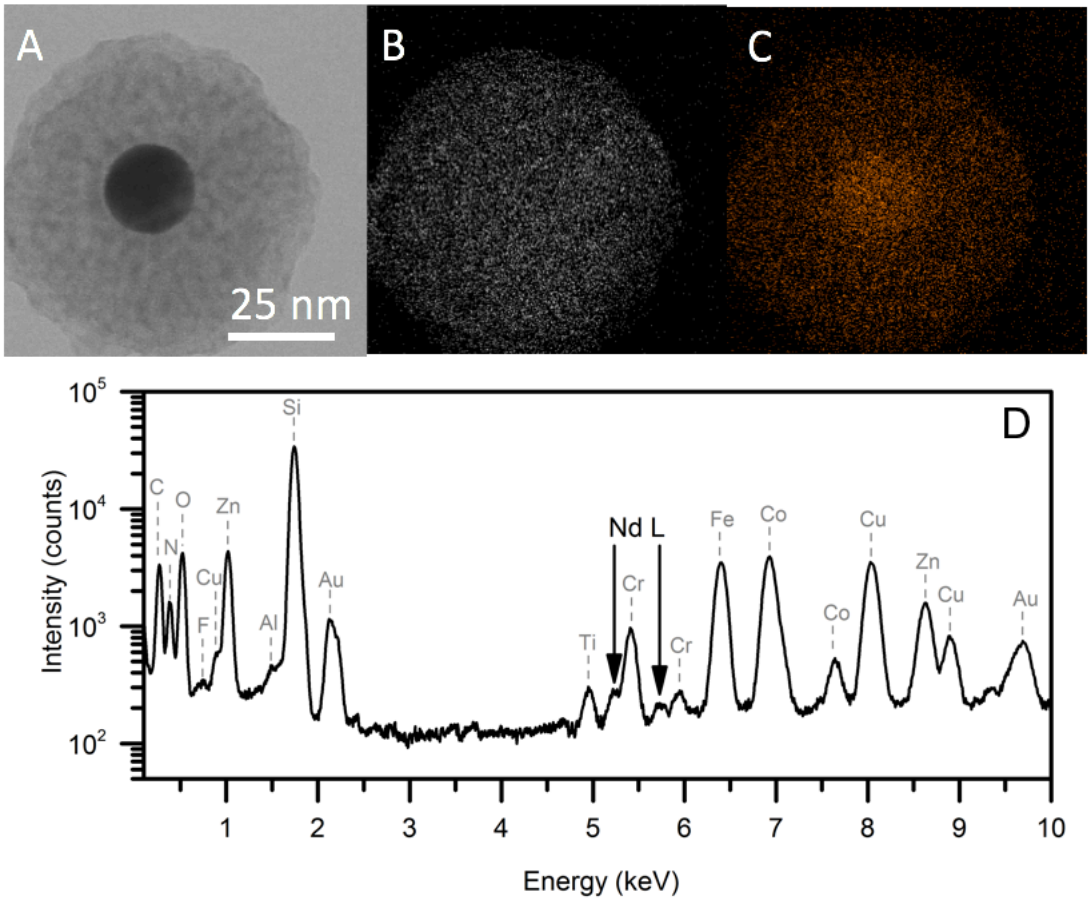

FIG. S13: Spatial correlation EDX-TEM for Nd-doped particles (pre-calcine) at 4%-added concentration (512x512). A) Greyscale TEM image, B) Spatial EDX map for Zn, C) Spatial EDX map for Nd. Color scale is enhanced for visual contrast in print. D) The corresponding spectrum, showing the presence of Nd.

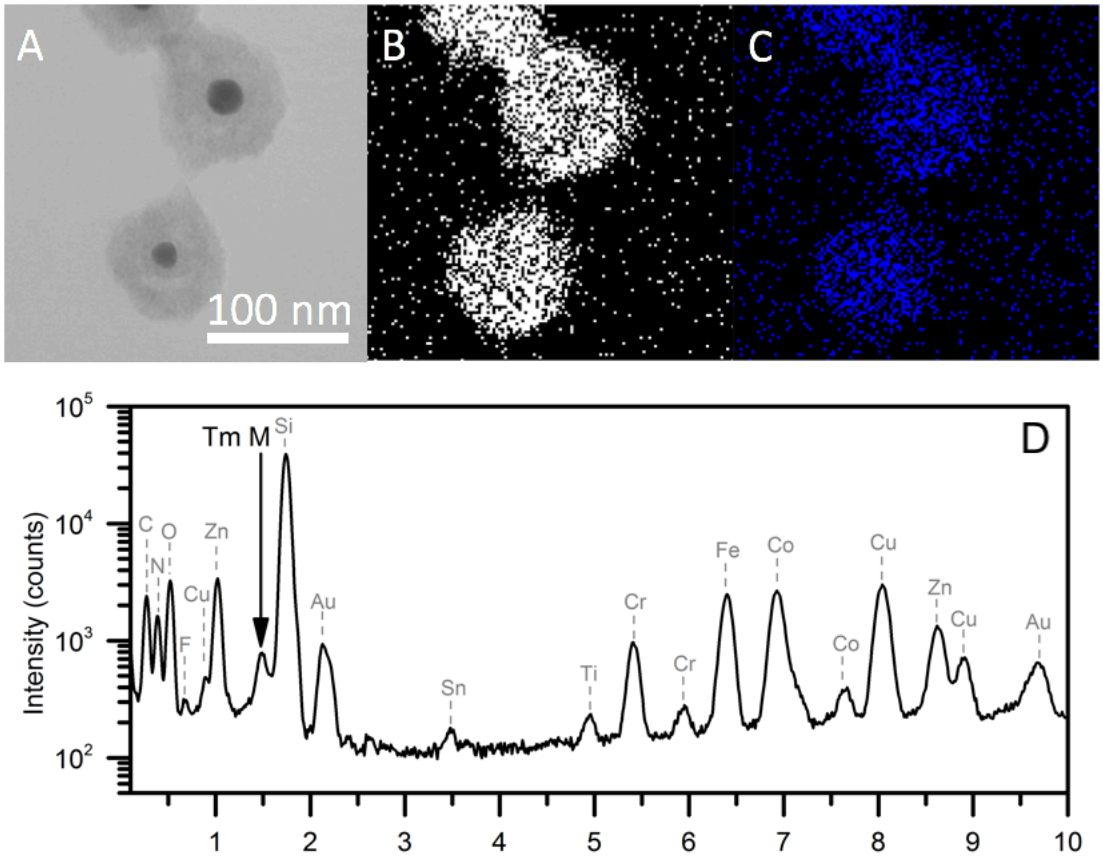

FIG. S14: Spatial correlation EDX-TEM for Tm-doped particles (pre-calcine) at 4%-added concentration (128x128). A) Greyscale TEM image, B) Spatial EDX map for Zn, C) Spatial EDX map for Tm. Color scale is enhanced for visual contrast in print. D) The corresponding spectrum, showing the presence of Tm.

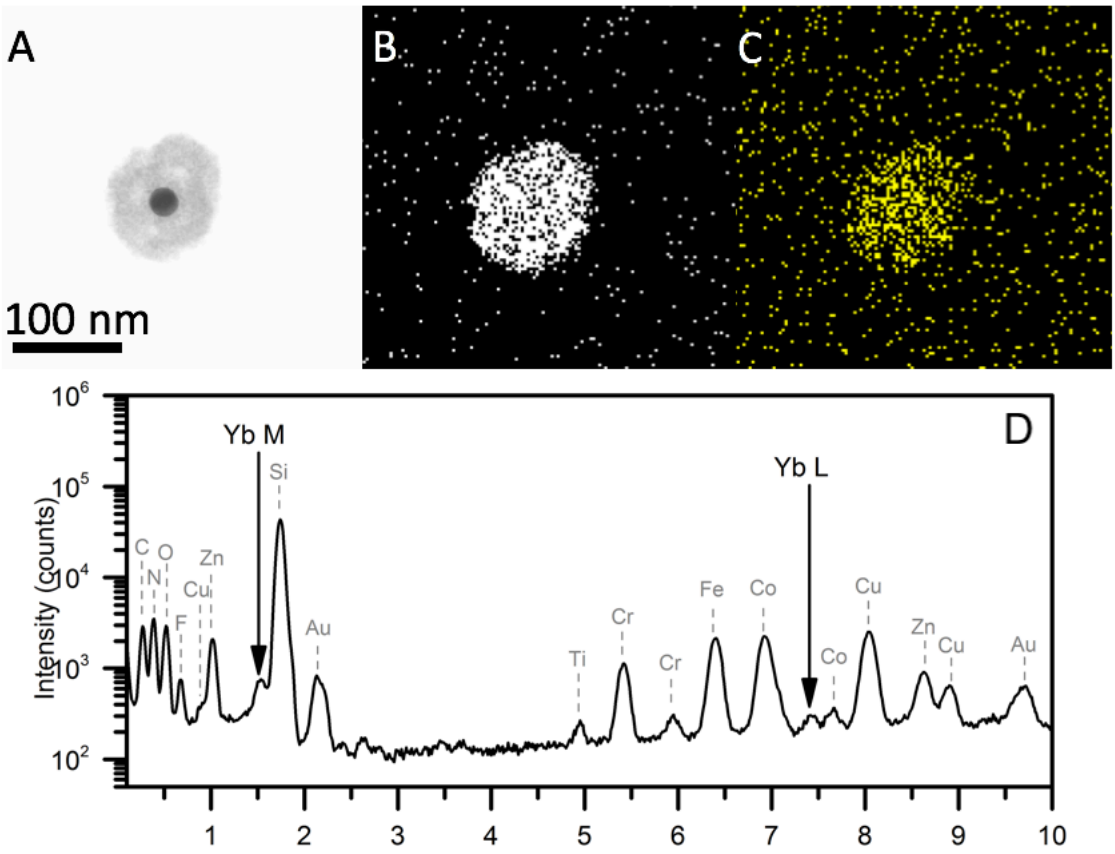

FIG. S15: Spatial correlation EDX-TEM for Yb-doped particles (pre-calcine) at 4%-added concentration (128x128). A) Greyscale TEM image, B) Spatial EDX map for Zn, C) Spatial EDX map for Yb. Color scale is enhanced for visual contrast in print. D) The corresponding spectrum, showing the presence of Yb.

Post-calcine particle analysis

In the past, it has been reported that the shell material is ZnO, implying crystalline ZnO, upon synthesis without the additional calcination treatment. Other studies have found it necessary to perform calcination first. However, the exact nature of the shell has never been previously characterized using methods like XRD. Therefore, the crystallinity of the shell is an open question in the field. Given that a key technical aspect of the present work is verifying the intercalation of the dopants into the ZnO shell, it is necessary to verify that the shell is ZnO. The crystalline nature of the shell with and without dopants was investigated using UV-Vis spectroscopy and XRD, and the impact on morphology was studied with SEM.

SEM analysis

Figure S16 is a collection of high-resolution SEM imaging done to qualitatively demonstrate the effect of calcining on the morphology of the particle. The images are of particles before and after calcining.

Since no EDX work was performed, these particles were able to be sputter coated with a thin layer of Pt:Pd to reduce charging and to enable higher resolution imaging. Images A, B, C, and D were taken at magnifications of 650kx, 250kx, 8000kx, and 500kx, respectively. There is no

apparent sintering, and the particles in the images correspond to the approximate size distributions we would expect from the DLS in Figures S1-S4.

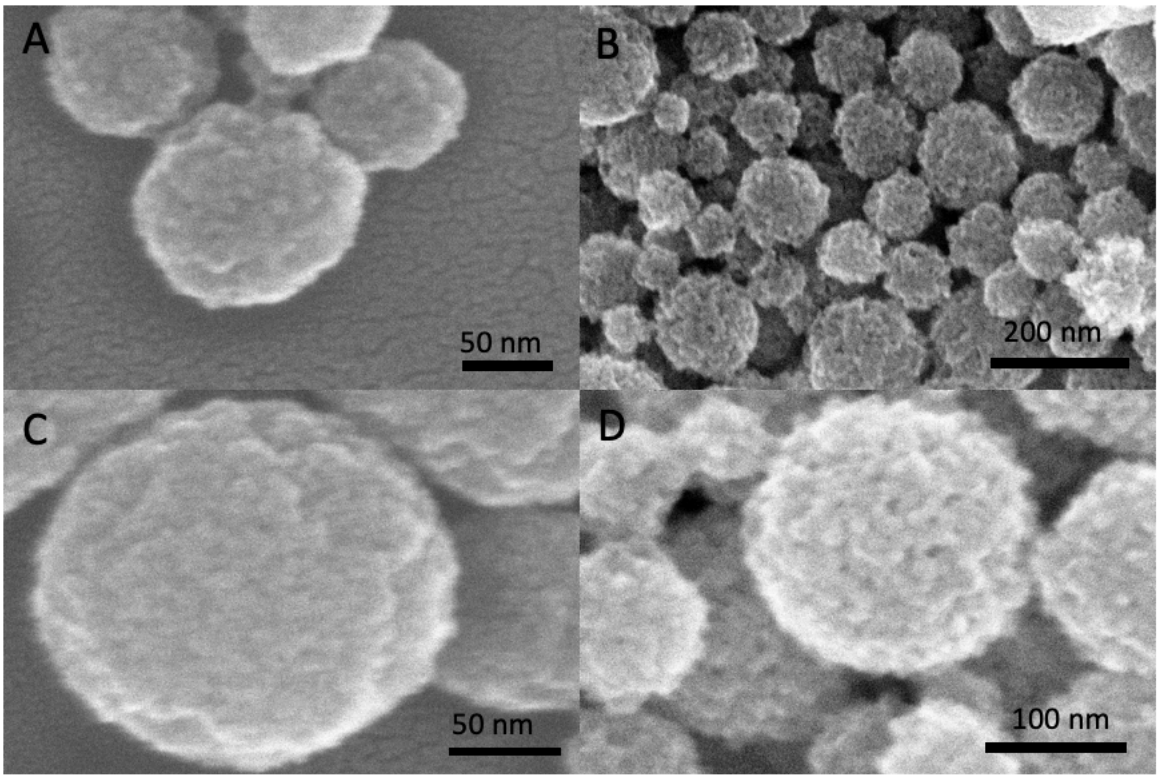

FIG. S16: High resolution imaging of A)-B) pre-calcined and C)-D) calcined ZnO particles. The particles still retain their spherical morphology.

X-Ray Diffraction (XRD) characterization

For the powder XRD study, 20 mL of samples containing each dopant (Cu, Ce, Er, Nd, Tm, Yb) at two different concentrations, 2% and 10% were prepared. The particle solutions were then purified and concentrated, deposited onto a Si/SiO_2 wafer (around 2 cm x 2 cm), and left to dry on a hot plate for 30 minutes. Each sample was placed in the powder XRD instrument and scanned from 5° to 60° (2θ angle) with an exposure time of 0.23 s and increment of 0.018° per exposure. The sample stage was also rotating at 15 RPM, and the beam power was 40 W on a copper x-ray emission tube (1.54 Å). After acquiring the pre-calcine XRD data, the samples were placed in a tube furnace and calcined. For all samples in this work, the calcination treatment involved heating at 500 °C in air for two hours, with a 15 minute ramp time, and natural air cooling after the treatment. The post-calcine samples were again scanned with the same parameters. The one exception was the 0% pre-calcine control scan, which had double the exposure time to be able to detect even faint amounts of ZnO present in the pre-calcine particles. The results are in Figures S17-S23.

There were 16 peaks that could be attributed to the nanoparticle, and these peaks are labeled with a letter (A-P) in each table on Figures S17-S23. First, several peaks associated with ZnO are present in all of the post-calcine, doped nanoparticle scans, and they are not present in the pre-

calcine scans. Additionally, in the 0% pre-calcine control scan which had additional scan time, there is very little (but detectable) ZnO formation, identified by the ZnO peaks I and K, at 31.5° and 34.2° respectively. These peaks were only identifiable after a longer exposure and are not present in the shorter exposure scans for the doped samples. Therefore, the calcining process is required for crystalline ZnO formation. Additionally, based on the width of the peaks, we conclude that the ZnO shell must be composed of small, randomly oriented ZnO grains.

Additionally, there are some new, but faint, peaks detected (A-G) in all of the pre-calcine scans. Properly identifying these peaks was outside of the scope of the experiment, but they are able to be reproduced, and clearly associated with the pre-calcine shell material, not any particular dopants. We believe they may be associated with zinc hydroxide formation and other pre-calcine shell material products.

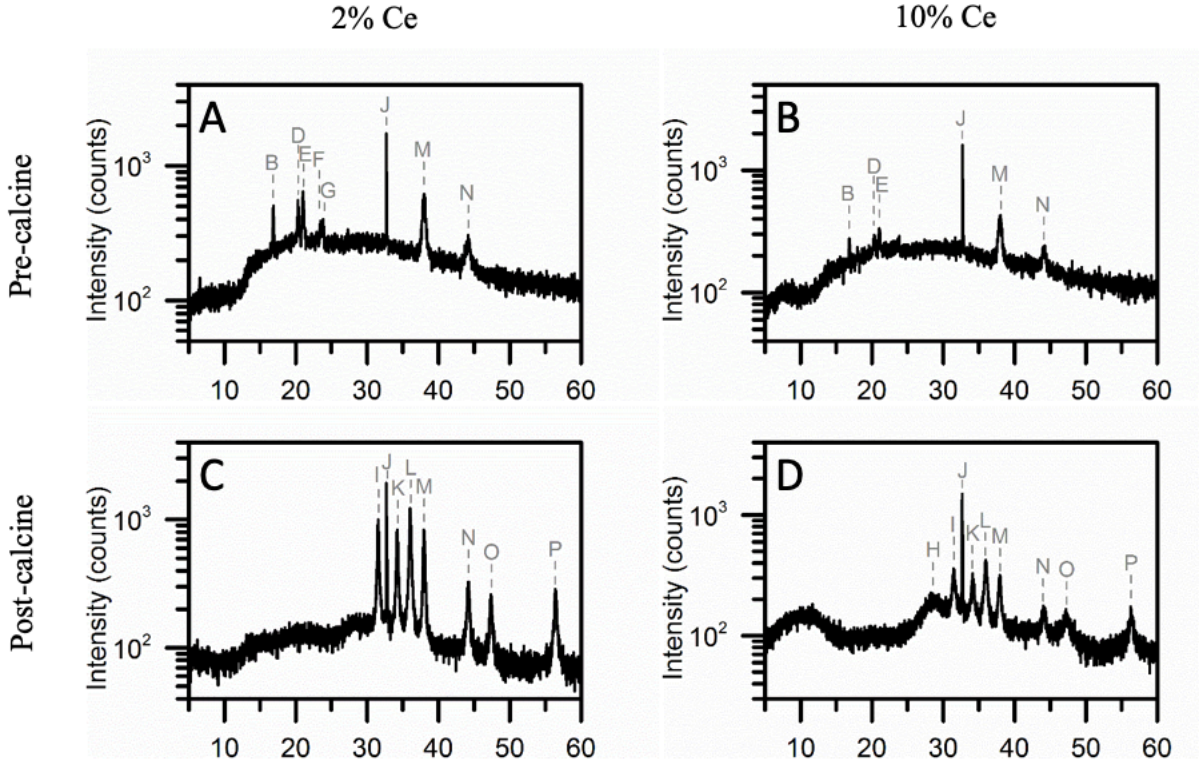

Peak	Angle	Association
A	8.8°	Pre-calcine shell
B	16.8°	Pre-calcine shell
C	17.9°	Pre-calcine shell
D	20.3°	Pre-calcine shell
E	21.0°	Pre-calcine shell
F	23.5°	Pre-calcine shell
G	23.8°	Pre-calcine shell
H	28.5°	CeO_2 phase
I	31.5°	ZnO shell
J	32.7°	Substrate
K	34.2°	ZnO shell
L	36.0°	ZnO shell
M	38.0°	Au core
N	44.1°	Au core
O	47.4°	ZnO shell
P	56.4°	ZnO shell

FIG. S17: Powder XRD patterns for core-shell nanoparticles doped with Ce. Left column: 2%, right column: 10%. Top row: pre-calcine, bottom row: post-calcine. Various weak peaks determined to be associated with the pre-calcine shell material are quenched during calcination, and the appearance of strong lines associated with ZnO occurs.

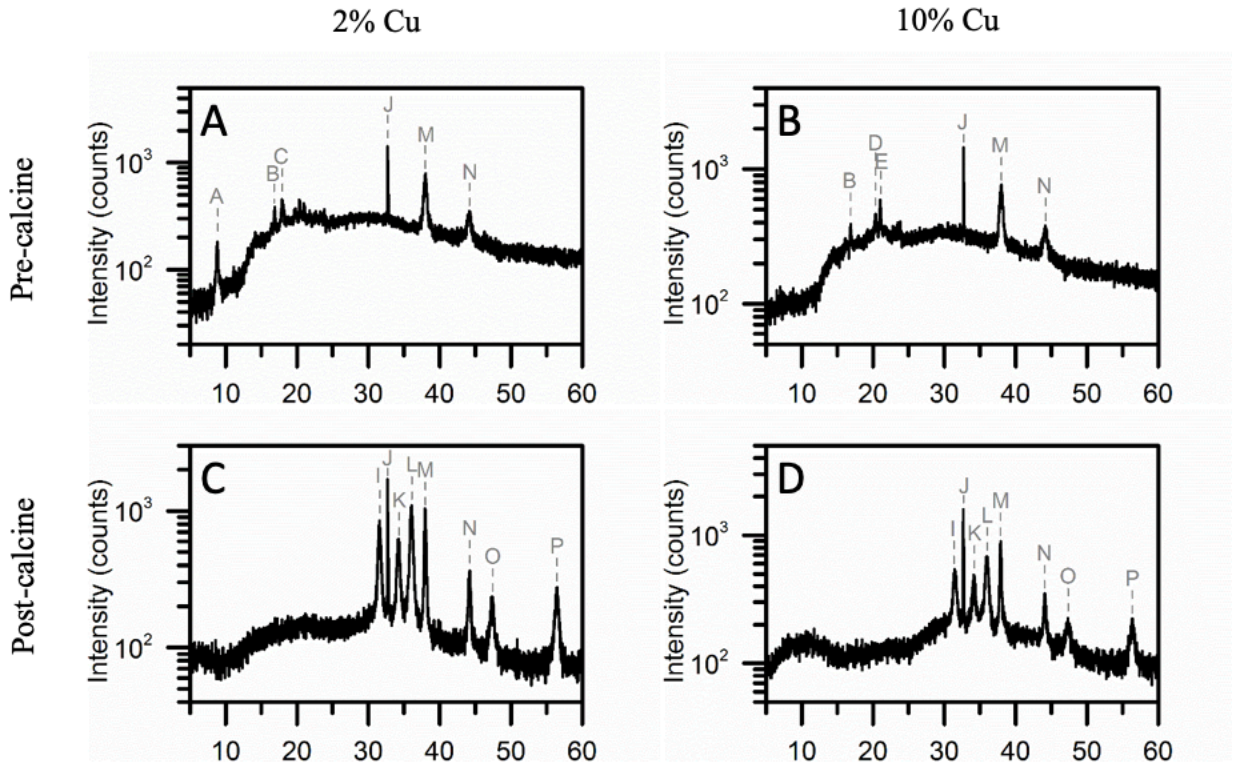

Peak	Angle	Association
A	8.8°	Pre-calcine shell
B	16.8°	Pre-calcine shell
C	17.9°	Pre-calcine shell
D	20.3°	Pre-calcine shell
E	21.0°	Pre-calcine shell
F	23.5°	Pre-calcine shell
G	23.8°	Pre-calcine shell
H	28.5°	CeO_2 phase
I	31.5°	ZnO shell
J	32.7°	Substrate
K	34.2°	ZnO shell
L	36.0°	ZnO shell
M	38.0°	Au core
N	44.1°	Au core
O	47.4°	ZnO shell
P	56.4°	ZnO shell

FIG. S18: Powder XRD patterns for core-shell nanoparticles doped with Cu. Left column: 2%, right column: 10%. Top row: pre-calcine, bottom row: post-calcine. Various weak peaks determined to be associated with the pre-calcine shell material are quenched during calcination, and the appearance of strong lines associated with ZnO occurs.

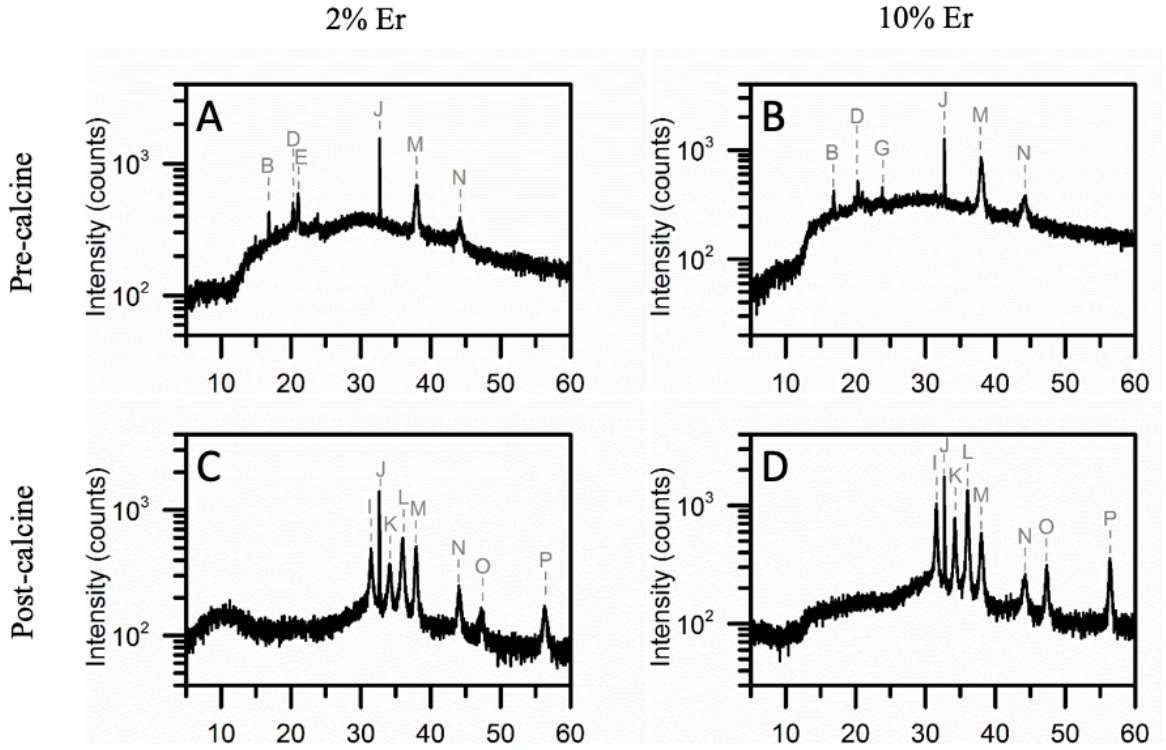

Peak	Angle	Association
A	8.8°	Pre-calcine shell
B	16.8°	Pre-calcine shell
C	17.9°	Pre-calcine shell
D	20.3°	Pre-calcine shell
E	21.0°	Pre-calcine shell
F	23.5°	Pre-calcine shell
G	23.8°	Pre-calcine shell
H	28.5°	CeO_2 phase
I	31.5°	ZnO shell
J	32.7°	Substrate
K	34.2°	ZnO shell
L	36.0°	ZnO shell
M	38.0°	Au core
N	44.1°	Au core
O	47.4°	ZnO shell
P	56.4°	ZnO shell

FIG. S19: Powder XRD patterns for core-shell nanoparticles doped with Er. Left column: 2%, right column: 10%. Top row: pre-calcine, bottom row: post-calcine. Various weak peaks determined to be associated with the pre-calcine shell material are quenched during calcination, and the appearance of strong lines associated with ZnO occurs.

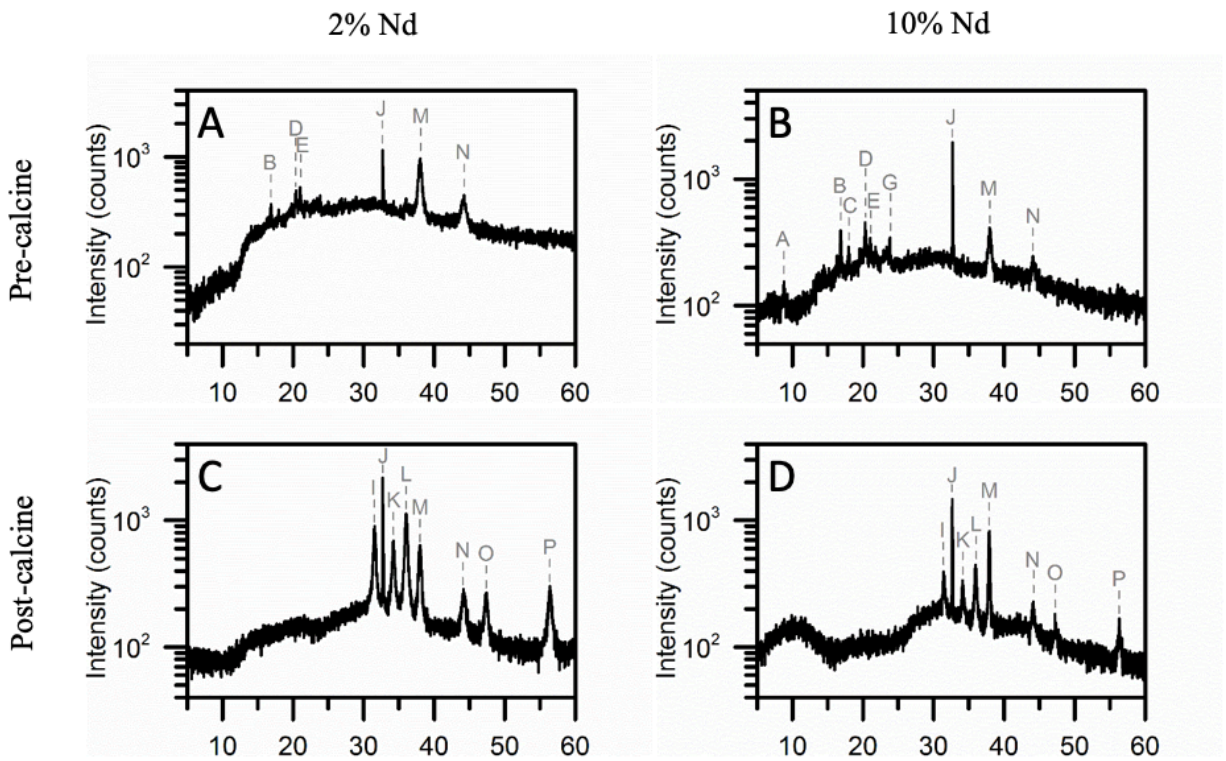

Peak	Angle	Association
A	8.8°	Pre-calcine shell
B	16.8°	Pre-calcine shell
C	17.9°	Pre-calcine shell
D	20.3°	Pre-calcine shell
E	21.0°	Pre-calcine shell
F	23.5°	Pre-calcine shell
G	23.8°	Pre-calcine shell
H	28.5°	CeO_2 phase
I	31.5°	ZnO shell
J	32.7°	Substrate
K	34.2°	ZnO shell
L	36.0°	ZnO shell
M	38.0°	Au core
N	44.1°	Au core
O	47.4°	ZnO shell
P	56.4°	ZnO shell

FIG. S20: Powder XRD patterns for core-shell nanoparticles doped with Nd. Left column: 2%, right column: 10%. Top row: pre-calcine, bottom row: post-calcine. Various weak peaks determined to be associated with the pre-calcine shell material are quenched during calcination, and the appearance of strong lines associated with ZnO occurs.

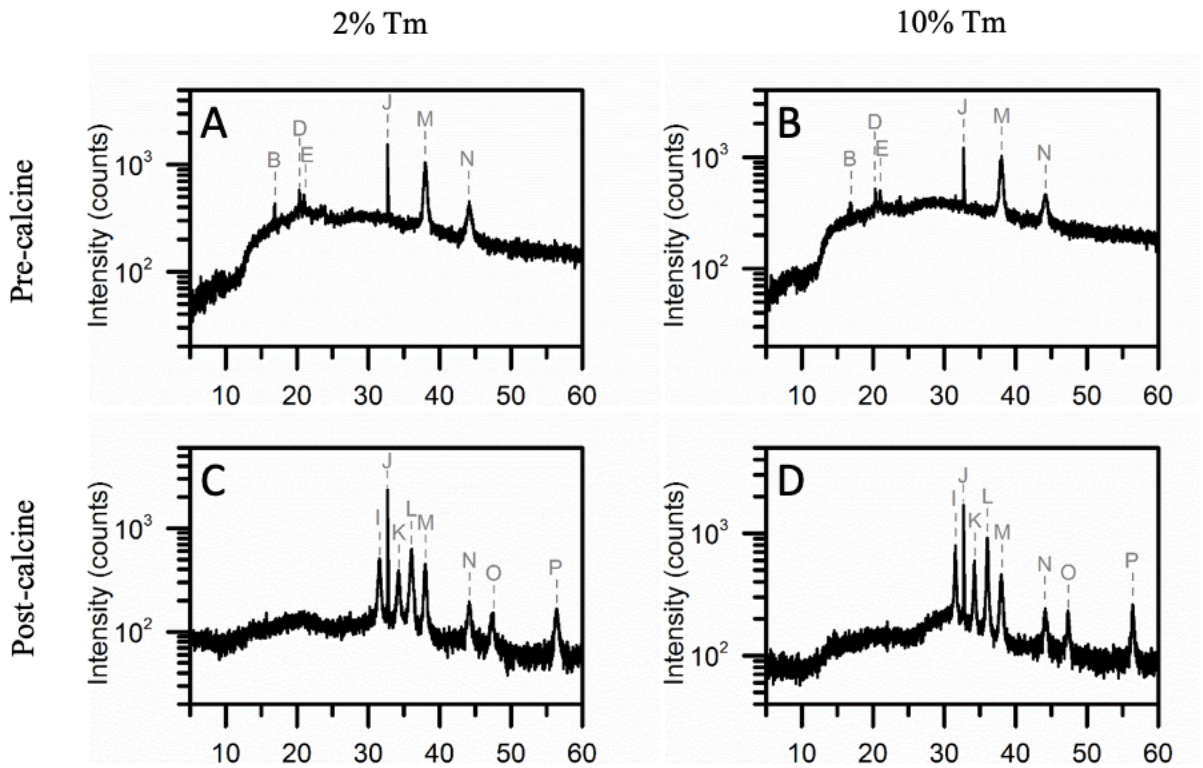

Peak	Angle	Association
A	8.8°	Pre-calcine shell
B	16.8°	Pre-calcine shell
C	17.9°	Pre-calcine shell
D	20.3°	Pre-calcine shell
E	21.0°	Pre-calcine shell
F	23.5°	Pre-calcine shell
G	23.8°	Pre-calcine shell
H	28.5°	CeO_2 phase
I	31.5°	ZnO shell
J	32.7°	Substrate
K	34.2°	ZnO shell
L	36.0°	ZnO shell
M	38.0°	Au core
N	44.1°	Au core
O	47.4°	ZnO shell
P	56.4°	ZnO shell

FIG. S21: Powder XRD patterns for core-shell nanoparticles doped with Tm. Left column: 2%, right column: 10%. Top row: pre-calcine, bottom row: post-calcine. Various weak peaks determined to be associated with the pre-calcine shell material are quenched during calcination, and the appearance of strong lines associated with ZnO occurs.

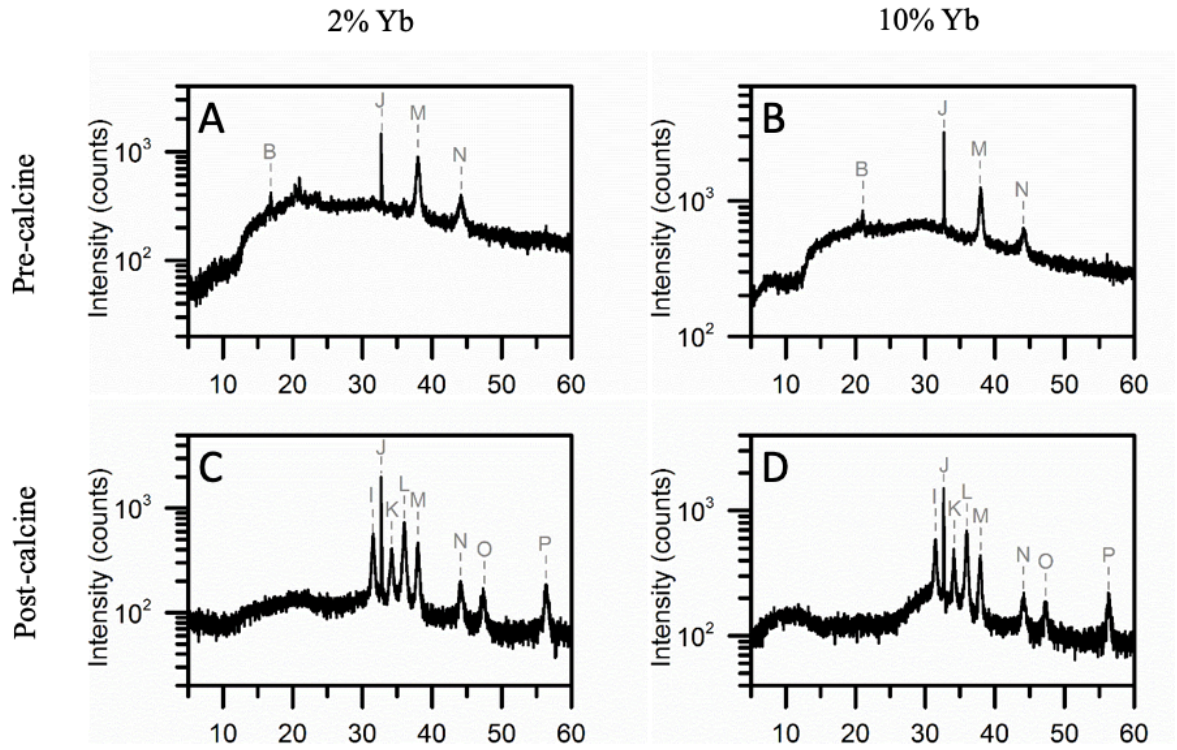

Peak	Angle	Association
A	8.8°	Pre-calcine shell
B	16.8°	Pre-calcine shell
C	17.9°	Pre-calcine shell
D	20.3°	Pre-calcine shell
E	21.0°	Pre-calcine shell
F	23.5°	Pre-calcine shell
G	23.8°	Pre-calcine shell
H	28.5°	CeO_2 phase
I	31.5°	ZnO shell
J	32.7°	Substrate
K	34.2°	ZnO shell
L	36.0°	ZnO shell
M	38.0°	Au core
N	44.1°	Au core
O	47.4°	ZnO shell
P	56.4°	ZnO shell

FIG. S22: Powder XRD patterns for core-shell nanoparticles doped with Yb. Left column: 2%, right column: 10%. Top row: pre-calcine, bottom row: post-calcine. Various weak peaks determined to be associated with the pre-calcine shell material are quenched during calcination, and the appearance of strong lines associated with ZnO occurs.

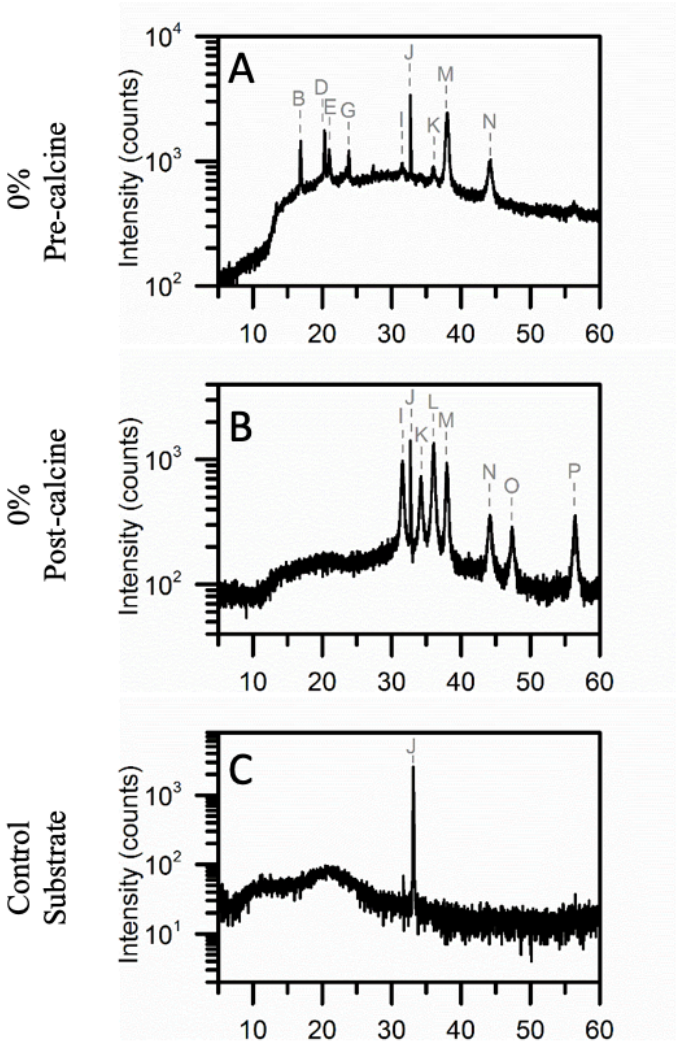

Peak	Angle	Association
A	8.8°	Pre-calcine shell
B	16.8°	Pre-calcine shell
C	17.9°	Pre-calcine shell
D	20.3°	Pre-calcine shell
E	21.0°	Pre-calcine shell
F	23.5°	Pre-calcine shell
G	23.8°	Pre-calcine shell
H	28.5°	CeO_2 phase
I	31.5°	ZnO shell
J	32.7°	Substrate
K	34.2°	ZnO shell
L	36.0°	ZnO shell
M	38.0°	Au core
N	44.1°	Au core
O	47.4°	ZnO shell
P	56.4°	ZnO shell

FIG. S23: Powder XRD patterns for control samples. 0% (undoped) core-shell nanoparticle on an SiO2/Si wafer, pre-calcine (top), and post-calcine (middle). Bottom: Bare SiO2/Si wafer pattern, showing the J peak which was present in all samples.

SEM analysis of Ce-doped particles

Figure S24 shows a pair of SEM images of the same sample and imaging location. The left image is a secondary electron image, and the right image is the backscattered electron image. The sample is 10% Ce-doped Au-ZnO nanoparticles, post-calcine, which was used for XRD data acquisition (shown in Figure 8 in the main text). This sample had a detectable CeO_2 phase present.

These images demonstrate the dramatic impact that 10% Ce-doping has on the structure of the particles. The secondary electron image shows the surface level morphology of the nanoparticles, which are no longer spherical (Figure S24A). The backscattered electron image penetrates deeper into the particles, showing strong contrast with the gold cores, indicating that these are core-shell nanoparticles (Figure 24B). The calcination treatment evidently did not significantly change the particles, based on similarity to other pre-calcine particles imaged at high Ce concentrations.

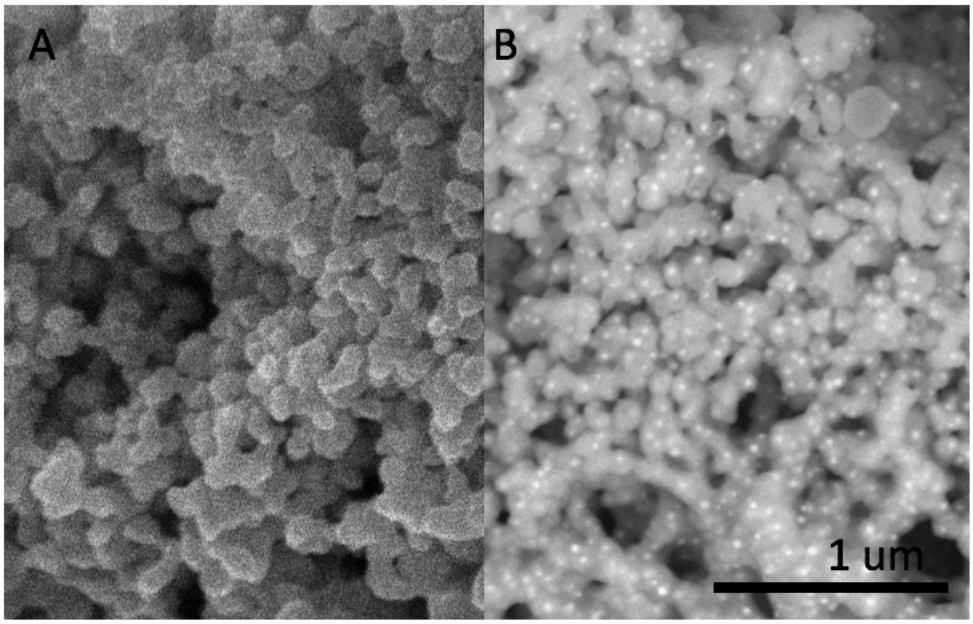

Figure S24: SEM imaging of Au-ZnO doped with 10%-added Ce, post-calcine. This sample was used for XRD analysis. Significant structural perturbations are evident. A) SE image, which emphasizes the external structure, B) CBS image of the same site, which emphasizes the internal structure, including the gold cores.